Journal of Environmental Chemical Engineering 4 (2016) 2458–2468

Contents lists available at ScienceDirect

Journal of Environmental Chemical Engineering

journal homepage: www.elsevier.com/locate/jece

Fe–Al binary oxide nanosorbent: Synthesis, characterization and phosphate sorption property

A.S. Tofik[a], Abi M. Taddesse[a,*], K.T. Tesfahun[a], G.G. Girma[b]

[a] Department of Chemistry, Haramaya University, Haramaya, Ethiopia
[b] Physics Department, Dire Dawa University, Dire Dawa, Ethiopia

ARTICLE INFO

Article history:
Received 17 December 2015
Received in revised form 15 April 2016
Accepted 17 April 2016
Available online 21 April 2016

Keywords:
Eutrophication
Nanosorbent
Fe-Al binary oxide
Adsorption
Phosphorus

ABSTRACT

Phosphorous removal using efficient treatment approach such as adsorption is vital for the control of eutrophication. In this study, nanosized Fe-Al binary oxide sorbent was synthesized through a modified gel evaporation method and employed for adsorption of phosphate from aqueous system. The nanosorbent was characterized by x-ray diffraction (XRD), scanning electron microscope coupled with energy dispersive x-ray spectroscopy (SEM/EDX), tunneling electron microscopy (TEM), Fourier transform infrared spectroscopy (FTIR) and flame atomic absorption spectroscopy (FAAS). Langmuir model showed the best fit to the experimental data with a maximum adsorption efficiency of 16.4 mg/g. Having all parameters optimized, it has been found that the nanosorbent exhibited 99.86% phosphate adsorption efficiency. The effect of co-existing anions on the adsorption of phosphate was also studied and no significant effect on the efficiency of the nanosorbent was observed due to competing ions such as fluoride. Desorbabilty of phosphate was investigated and found to be increased with increasing pH. The results of thermodynamic studies indicated that the process is spontaneous and endothermic. Both macroscopic and microscopic approaches were employed to predict the mechanism of phosphate adsorption on the Fe-Al binary oxide nanosorbent. Accordingly, the phosphate adsorption is presumed to occur via the replacement of surface hydroxyl groups by the phosphate species and formation of inner-sphere surface complexes at the water/oxide interface.

1. Introduction

Phosphorus has been regarded as a limiting nutrient responsible for eutrophication of water bodies. The presence of trace amount of phosphate (even less than 1 ppm) in treated wastewater is often responsible for eutrophication; particularly in lakes and slow moving rivers [1]. Therefore, removing phosphate is very important before discharging wastewater into the water environment.

Several techniques have been developed for P removal which includes chemical precipitation [2], biological removal [3], reverse osmosis [1], electrodialysis [4], ion exchange [5], constructed wetlands [6] and adsorption [7,8]. Among these available approaches, chemical precipitation and biological removal in general are not able to meet the stringent effluent standards while ion exchange, electrodialysis and reverse osmosis require high investment and operation costs. Compared with these techniques, adsorption methods proved to be more promising due to their low cost, effective treatment in dilute solutions, and high uptake capacity. Another attractive feature of this technique is that the nutrient-loaded filters can be used in agriculture as phosphate fertilizers [9]. This particular feature is important since phosphate is recognized as one of the natural resources that could possibly be exhausted in the near future [10].

A large number of materials from natural minerals to synthetic ones have been used as adsorbents to adsorb phosphate from wastewater. These adsorbents include minerals [11], soils [12], industrial by-products [13–16,54], and synthetic products [17–19]. Considerable number of reports has shown that excellent and efficient phosphorus adsorbents are all characterized by their high iron, alumina, calcium and manganese contents [20–25]. Thus, substrates with high contents of these materials can be efficient phosphate sinks in immobilizing phosphate from soils and water bodies.

Mixed metal oxides exhibit surface properties that mimic the natural systems more closely than their individual components. Multi-component sorbents demonstrate physico-chemical properties significantly different from those of their single counter

* Corresponding author at: P.O.Box 90, Haramaya University Haramaya, Ethiopia.
E-mail address: abi92003@yahoo.com (A.M. Taddesse).

http://dx.doi.org/10.1016/j.jece.2016.04.023
2213-3437/

parts. It is these differences in physico-chemical properties that are considered to be the major reasons for differences in sorption behavior between multi- and single-component systems [20]. For example, increased fixation of Cu and Pb in Fe/Al oxide system (compared to single counter parts) is attributed to increased surface area and surface charge [26,27]. Although sorption characteristics of single component Al or Fe hydr (oxides) have been widely studied, limited work has been conducted on the sorption characteristics of mixed Al–Fe binary oxide especially at nanoscale.

Adsorbents synthesized with iron oxide that incorporate different metal ions for high adsorption performance have been studied. Al (III), Cr (III), Cu (II), Mn (IV), Ti (IV) and Zr (IV) [28–33,51] ions had been introduced into iron oxide to form bimetallic/trimetalic oxide adsorbents for phosphate sorption. Among these mixed oxides Fe-Cu, Fe-Zr and Ti-Fe binary oxides have been prepared in crystalline form where as the remaining are amorphous. Reports documented in relation to phosphate sorption using Fe-Al binary oxides are all in amorphous forms though crystalline forms of the oxyhydroxides are reported for photocatalytic applications [34,35]. Hence, there is still a dearth of information related to the synthesis, characterization and sorption property studies of Fe-Al binary mixed oxide in nanocrystalline form for phosphate removal from wastewater. Recently, materials with nanostructure have gained special attention in the field of solute adsorption from the liquid phase due to small particle size, large surface area to volume ratio, high *in situ* reactivity and absence of diffusion resistance [36,37].

In the present work, we report the synthesis and phosphate sorption behavior of nanocrystaline Fe-Al binary oxide sorbent. The synthesis involved a series of Fe–Al binary oxides with different Fe/Al ratios (from 0 to 30%) and the binary system with the smallest size was selected and tested for phosphate adsorption study. The adsorption kinetics, adsorption isotherms and desorption studies have been carried out. Additionally, the influence of operating parameters such as solution pH, ionic strength and coexisting anions on phosphate adsorption were investigated. Phosphate adsorption mechanism was also elucidated in the present paper based on macroscopic and microscopic approaches. The as-synthesized Fe-Al nanosorbent exhibited potentially high (99.86%) phosphate adsorption efficiency. The effect of co-existing anions on the adsorption of phosphate showed no significant effect making the material a promising sorbent for phosphate sorption from aqueous systems in the presence of interfering ions.

2. Methodology

2.1. Synthesis of the nanosorbent

Gel evaporation method [38] with some modifications was followed to synthesize Fe-Al binary oxide nanosorbent. The percentage of aluminum in the binary systems varied from 0 to 30%. The starting materials [ferric nitrate nonahydrate Fe $(NO_3)_3{\cdot}9H_2O$ and aluminum nitrate nonahydrate Al $(NO_3)_3{\cdot}9H_2O$] were dissolved in ethylene glycol at a molar ratio of (total metal nitrates: ethylene glycol = 1:3) with the addition of a minimum volume of water enough to dissolve the nitrates. The resulting solution was warmed on hot plate stirrer at 90 °C to evaporate the solvents, after which the nitrate glycol mixture auto-ignited, producing voluminous foam and finally yielding a loose powder. The powders were dry ground and calcined at three different temperatures: 300 °C, 600 °C and 900 °C for 5 h. The as synthesized powders were designated according to the Al content and temperature of calcinations. For example, the mixed oxide containing 0% Al calcined at 300 °C was designated as 0Al300, and so on. A total of nine samples were synthesized and based on the XRD results, the sample with the smallest crystalline size was selected for the subsequent sorption experiment.

2.2. Elemental analysis

The percentage of iron as iron oxide in all the as-synthesized powders was determined by flame atomic absorption spectrophotometer (AAS). 0.5 g of the as-synthesized powders was digested with concentrated nitric acid (7 mL), concentrated hydrochloric acid (4 mL) and hydrogen peroxide (2 mL) using acid digestion tube till clear solution appeared. The samples were transferred to 100 mL volumetric flasks and brought to volume using deionized water. 1 mL of this solution was diluted further to 50 mL and the concentration of iron was read from the solution in 50 mL volumetric flasks using AAS [20].

2.3. Characterization of the as-Synthesized powder

X-ray diffraction (XRD) analysis of the synthesized particles was made using an x-ray powder diffractometer (Philips Analytical PW-1710) equipped with Cu Kα radiation (λ = 0.1541 nm) at a scan speed of 2°/min from 10° to 80°, operated at voltage 40 kv and applied potential current 30 mA. The average crystallite size was determined from the XRD peaks using Debye-Scherrer equation and the sample with the smallest size was selected for the subsequent sorption studies. The surface morphology of the prepared adsorbent was observed by scanning electron microscopy (SEM) using JSM-6700F LV microscope. The elemental composition of the sample was further analyzed by energy dispersive analysis system using EDX GENESIS (EDAX, Ltd., USA). Transmission electron micrographic (TEM) images were recorded on a H800 transmission electron micrograph (Hitachi, Japan). The IR spectra of the prepared adsorbent before and after phosphate adsorption were measured by a Fourier transform infrared spectrometer (SHIMADZU 1730, Japan).

2.4. Batch adsorption studies

Batch mode adsorption studies for phosphate were carried out in 50 mL Erlenmeyer flask. The batch adsorption process was optimized with respect to pH, adsorbent dose, speed of agitation, contact time and initial phosphate ion concentration. For each run, the resulting suspension of the phosphate ions was filtered using a Whatman No.1 filter paper and the filtrate was analyzed calorimetrically for the corresponding phosphate ion concentration. Removal efficiency was finally calculated by using the relationship given below.

$$\text{Adsorption}\% = \frac{C_o - C_f}{C_o} x100 \quad (1)$$

where C_o = the initial concentrations (mg/L) and C_f = final concentrations (mg/L) of the phosphate ion.

The adsorption capacity of the phosphate ion is the concentration of the phosphate ion on the adsorbent mass and was calculated based on the mass balance principle,

$$q_e = \frac{C_o - C_f}{m} xV \quad (2)$$

where: q_e = adsorption capacity of adsorbent (mg/g), V = the volume of reaction mixture (L), m = the mass of adsorbent used (g), C_o = the initial concentrations (mg/L) and C_f = final concentrations (mg/L) of the phosphate ion.

2.4.1. Effect of pH and ionic strength

To gain insight into the adsorption process, the influence of pH was studied as follows. Solutions containing 30 mg/L of phosphate

were adjusted with HCl and NaOH solutions to the desired pH values from 2 to 9. The other parameters such as adsorbent dose, agitation speed and contact time were kept constant. Effect of ionic strength was studied taking the initial phosphate concentration of 5 mg/L. The solution pH was adjusted from 2 to 10, the concentrations of $NaNO_3$ were 0.1, 0.01, 0.001 M, respectively, and the contact time was 8 h.

2.4.2. Effect of adsorbent dosage

The effect of adsorbent dosage was studied by using 0.05, 0.075, 0.1, 0.5, 1 and 2 g of the adsorbent in 50 mL Erlenmeyer flask with phosphate ion concentration of 30 mg/L and the adsorption efficiency for each dose was determined by keeping other parameters (pH, agitation speed, contact time and initial phosphate concentration) constant.

2.4.3. Effect of agitation speed

In this study, the effect of varying the agitation speed was investigated by keeping the other operating parameters (pH, adsorbent dose, contact time and initial phosphate concentration) constant. A series of experiments was undertaken with different agitation speeds: 50, 100,120 140, 160 and 200 rpm.

2.4.4. Effect of contact time

The effect of contact time on phosphate sorption was determined by varying the contact time to 3, 6, 12, 16, 24 and 48 h with the other parameters (pH, adsorbent dose, agitation speed and initial phosphate concentration) kept constant.

2.4.5. Effect of phosphate ion concentration

The effect of phosphate concentration was determined considering the following initial phosphate ion concentration: 10, 20, 30, 50, 100, 150 and 200 mg/L keeping other parameters (pH, adsorbent dose, and agitation speed and contact time) constant.

2.4.6. Adsorption isotherms

Adsorption isotherms are mathematical models that describe the distribution of the adsorbate species among the liquid and solid phases based on a set of assumptions that are related to the heterogeneity or homogeneity of the solid surface, the type of coverage, and the possibility of interaction between the adsorbate species. In order to construct adsorption isotherms for the adsorbent, experiments were carried out by varying the initial phosphate ions concentration from 10 to 200 ppm and with the adsorbent dose of 0.1 g.

2.4.7. Selectivity of phosphate adsorption

The dependency of phosphate adsorption onto the as-synthesized powder in the presence of other anions which are commonly present in water namely F^-, SO_4^{2-}, HCO_3^- and NO_3^- was investigated. 20 mg/L of these anions were prepared from NaF, Na_2SO_4, $NaHCO_3$ and $NaNO_3$. The effect of mixture of anions and also the effect of individual anions were studied to estimate the selective adsorption of phosphate.

2.4.8. Thermodynamic study

Thermodynamic parameters shed valuable insight into feasibility and spontaneity nature of the adsorption process [54]. By plotting the graph $\ln K_c$ versus T^{-1}, the values of ΔH and ΔS were estimated from the slopes and intercepts and on the basis of this, the spontaneity of the process was assessed. Based on the above approach, the free energy change (ΔG), enthalpy change (ΔH) and entropy change (ΔS) were calculated for the sorbent.

2.4.9. Kinetic studies

Adsorption is time dependent process and it is very important to know the rate of the process and evaluate the adsorbent in removing phosphate from aqueous system. Kinetic models based on the capacity of the adsorbent have been investigated, such as the Lagergren's first-order equation and Ho's second-order expression [39,40]. The first-order equation of Lagergren and the pseudo second-order equation are the most widely used kinetic models to describe the sorption process. First-order rate expression of Lagergren considers that the rate of occupation of adsorption sites is proportional to the number of unoccupied sites. The Lagergren model proposed in 1898 assumes a first order adsorption kinetics and can be represented by the equation:

$$\frac{dq_t}{dt} = k_1(q_e - q_t) \quad (3)$$

where, k_1 is the rate constant for pseudo-first order adsorption, q_e and q_t are the amount of phosphate adsorbed (mg/g) at equilibrium and at any time t, respectively. This equation can be integrated to yield a linearzed form at initial condition $q_t = 0$, $t = 0$ and $q_t = t$ and $t = t$.

$$\log(q_e - q_t) = \log q_e - \frac{K_1}{2.303}t \quad (4)$$

In this equation, the rate of adsorption is assumed to be proportional to the difference between the adsorption capacity at equilibruim (q_e) and the adsorption capacity at time t (q_t). The pseudo- first order kinetics is applicable if the plot of log ($q_e - q_t$) against t shows linear relationship. A straight line plot of log ($q_e - q_t$) versus t was used to determine the first order rate constant, k_1 and the adsorption capacity, q_e.

The pseudo second order rate equation is expressed as:

$$\frac{dq_t}{dt} = k_2(q_e - q_t)^2 \quad (5)$$

where, k_2 is equilibrium rate constant of second order kinetics model ($g\,mg^{-1}\,h^{-1}$). For boundary condition $t = 0$ to $t = t$ and $q_t = 0$ to $q_t = q_e$, the integrated form of the equation becomes

$$\frac{1}{q_e - q_t} = \frac{1}{q_e} + k_2 t \quad (6)$$

Then, the linearized form is:

$$\frac{t}{q_t} = \frac{1}{K_2 q_e^2} + \frac{t}{q_e} \quad (7)$$

The pseudo-second order rate constant (k_2) and the equilibrium adsorption capacity (q_e) can be determined experimentally from the slope and intercept of the plot t/q_t versus t. The plot t/q_t versus t should give a straight line if pseudo-second order kinetics is applicable. The kinetics of adsorption study was carried at initial phosphate concentration of 20 mg/L with corresponding adsorbent dose of 0.1 g. The residual concentrations were measured at different time intervals.

2.4.10. Desorption of phosphate

Phosphate desorption was studied using phosphate loaded powder sample [41]. The powder was immersed in the regenerating solution and placed in shaker at 25 °C for 12 h. To this, 0.1 M NaOH solution was used to effect the desorption. The desorbed adsorbate in the solution was finally recovered by filtration and analyzed for the corresponding phosphate ion concentration. The recovery percentage was obtained from the following relation.

$$\text{Desorption Efficiency}\% = \frac{\text{Desorbed}}{\text{Adsorbed}} \text{x} 100 \quad (8)$$

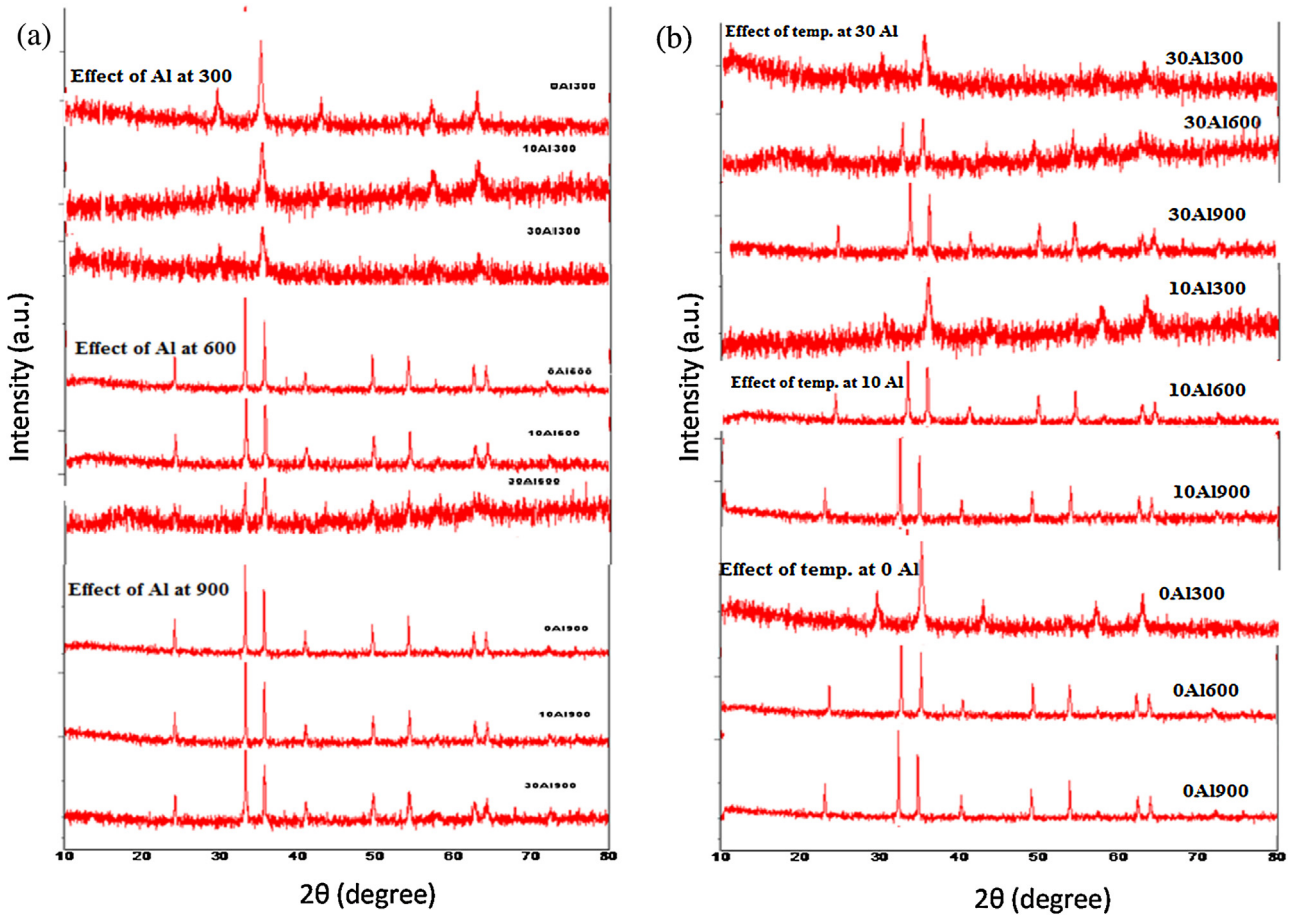

Fig. 1. Effect of Al content (a) and temperature (b) on the XRD patterns of the as-synthesized powders.

where, Desorbed = the concentration and/or the mass of the phosphate ion after the desorption process, Adsorbed = (Co – Ce) for each recovery process.

2.4.11. Analysis of phosphate

The analysis of phosphate was done spectrophotometrically using molybdenum blue method [42]. This involves reaction of phosphate ions with an acid solution containing molybdate and antimony ions to form an antimony phosphomolybdate complex followed by reduction of this complex with ascorbic acid to form a strongly colored molybdenum blue complex. The intensity of the blue color correlates to the concentration of phosphate. Concentrated solutions were diluted prior to determination and corrected with dilution factor.

3. Results and discussion

3.1. XRD

After calcinations at 300 °C, 600 °C and 900 °C, the crystalline phases in the samples were determined from the XRD patterns using the relevant ICDD data to investigate the structural changes caused by thermal treatment and alumina incorporation. At 300 °C, the peaks observed at 2θ values of 31, 36, 43, 56.5, and 63 for the sample 0Al300 could be attributed to maghemite (Fig. 1a).

For the same sintering temperature, the peaks started to diminish with increasing alumina content from 10% to 30% indicating that increasing the alumina content decreases crystallinity (Fig. 1a). At 600 °C, more peaks are observed that were not distinct at 300 °C for all iron alumina combination carried out under this study. The peaks at 2θ values of 24, 33, 36, 41, 49.5, 55.6 and 64 correspond to hematite and the remaining peaks correspond to maghemite (Fig. 1a). At this temperature as well, the degree of crystallinity of iron oxide decreased with increasing alumina. At 900 °C, the peaks at 2θ values corresponding to 24, 33, 36, 41, 49.5, 54.5, 63, 64.5, 72.5 are all associated with hematite (Fig. 1a). Increasing calcination temperature therefore increases crystal transformation of iron oxides from maghemaite to hematite significantly. The presence of alumina delays not only crystallization but also transformation from maghemite to hematite (Fig. 1b). The observed effect of thermal treatment and alumina incorporation to iron oxide in our study is similar to previous reports [34–36]. No any peak presented was attributable to alumina in our result implying that alumina should be amorphous structure. In fact, crystallized alumina such as γ-Al_2O_3 might present under thermal treatment at 800 °C, but the amount may not be good enough to bring about this change at the concentration used in this

Table 1
Crystal size and percentage of Fe_2O_3 for the as-synthesized nanosorbent.

Adsorbent	2θ(degree)	β (degree)	D(nm)	Percentage of Fe_2O_3
0Al300	35.516	0.355	23.5	97.5
0Al600	33.207	0.225	36.87	97.5
0Al900	33.237	0.223	37.2	97.8
10Al300	35.827	0.399	20.94	91.8
10Al600	33.361	0.217	38.19	86.1
10Al900	33.347	0.209	39.72	86.1
30Al300	35.978	0.340	24.58	74.1
30Al600	35.870	0.265	31.68	69.0
30Al900	33.407	0.272	30.5	69.0

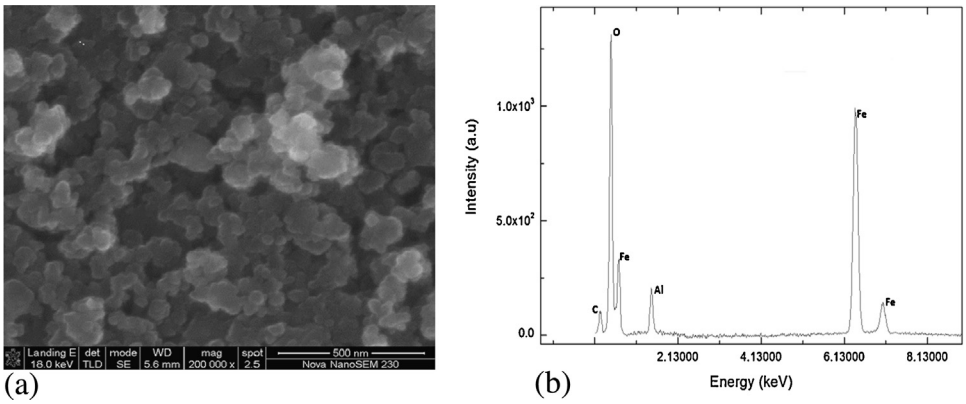

Fig. 2. a) Scanning electron microscopic image of 10Al300 b) EDX spectrum of 10Al300.

experiment that is 30%. This is evidenced by the finding of [34], who observed peaks representing alumina at concentration higher than 30% for a temperature above 600 °C.

The average crystalline size was estimated using Debye Scherrer equation [43]

$$D = \frac{K\lambda}{\beta Cos\theta} \quad (9)$$

where, D is crystallite size in nm, K is the shape factor constant usually 0.9, β is the full width at half maximum(FWHM) in radians of 2θ, λ is the wavelength of the X-ray which is 0.15406 nm for Cu target $K\alpha_1$ radiation and θ is the Bragg's angle.

The calculated crystallite size is shown in Table 1. The as-synthesized powders ranged from 20 to 40 nm. The average Fe_2O_3 contents in the three samples was roughly 98%, 89% and 71.5% for 0%, 10% and 30% addition of Al_2O_3 in the samples. The iron oxide content is consistent with the theoretical value expected in the samples. The difference from the theoretical value seemed to increase with increasing sintering temperature which could be accounted to the loss of the sample by carry over effect. As can be seen from Table 1, sample 10Al300 exhibited the smallest crystalline size and this sample was selected for the sorption experiment. Further characterization by SEM-EDX, TEM and FTIR to extract more information with respect to morphology, crystallite size and functional groups was also made on the selected nanosorbent named here after as Fe-Al binary oxide nanosorbent.

3.2. SEM-EDX

Scanning electron microscopy coupled with energy dispersive X-ray detector (SEM-EDX) was used to observe the morphology, particle size and composition of Fe-Al binary oxide nanosorbent. Sample 10Al300 was selected due to the smallest crystallite size obtained from XRD. SEM micrographs (Fig. 2a) corroborate the presence of homogenous particle size distribution with particle size below 100 nm. X-ray energy dispersive analysis of the imaged area (Fig. 2b) shows a relative concentration of aluminum and iron of 2.75% and 27.64%, respectively.

3.3. TEM

Further confirmation of the actual particle size was obtained by TEM studies. Fig. 3 show representative images of 10Al300 Fe-Al binary oxide nanosorbent. The material is formed by agglomerates of nanoparticles. The particle size distribution ranged from 8 to 20 nm with a maximum average crystallite size of 12 nm (Fig. 3b). These values agree less with those calculated from Debye-Scherrer formula (20.9 nm) which looses accuracy as the particle size

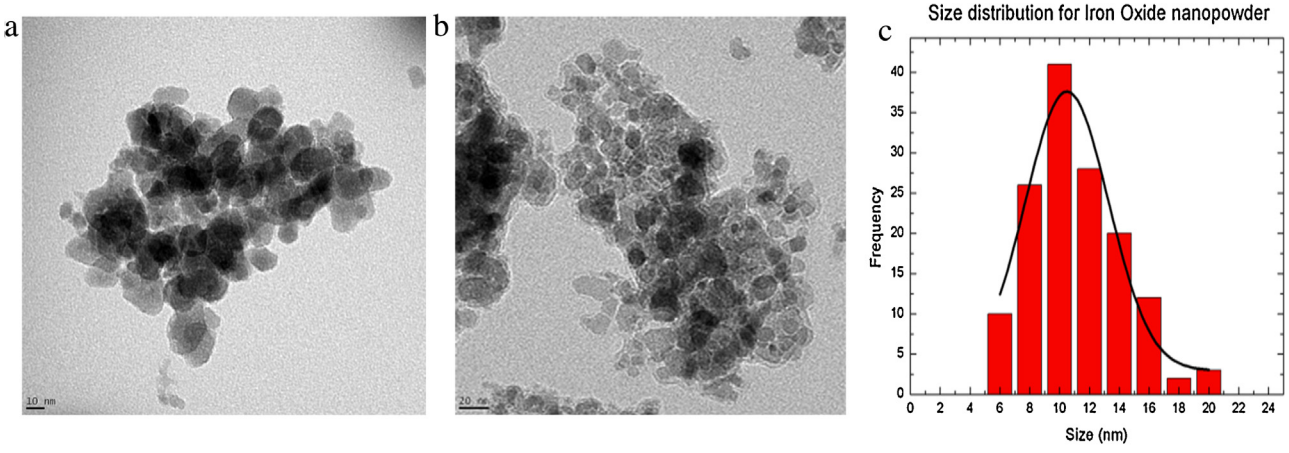

Fig. 3. TEM images (a &b) and particle size distribution (c) of 10Al300.

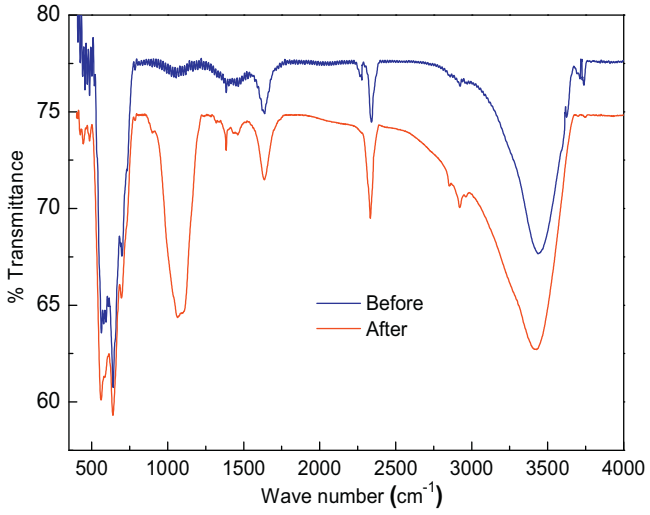

Fig. 4. FTIR spectrum of 10Al30 before and after phosphate sorption.

decreases. Nevertheless, electron microscopy studies confirmed that the as-synthesized material is in the nano-range.

3.4. FTIR

The IR spectra of 10Al300 display a number of peaks before and after phosphate adsorption (Fig. 4). The peaks observed in both cases are more or less similar. The absorption bands observed from 3400 to 3500 cm^{-1} represent O—H stretching vibrations of adsorbed water molecules. The peaks observed at 1620 cm^{-1} can be ascribed to bending modes of water molecules. The absorption band at 2310 cm^{-1} is also common to both spectra which could be assigned to the adsorbed carbonate, because the adsorption tests were carried out open to the atmosphere. The absorption bands observed at 1340 cm^{-1} and 1114 cm^{-1} could be attributed to surface and multi-centered hydroxyl groups respectively. The M—O stretching frequencies are observed at absorption bands of 660 cm^{-1} and 560 cm^{-1}. For a spectrum after phosphate adsorption additional peak at 1078 cm^{-1} was observed owing to the P-O stretching modes indicating the adsorption of phosphate on the surface of the nanosorbent [29]

3.5. Effect of ionic strength

The phosphate adsorption mechanism of Fe-Al binary oxide nanosorbent was investigated by evaluating the ionic strength effect on the adsorption behavior. Fig. 5 demonstrates that the phosphate adsorption showed no significant change on phosphate adsorption as the ionic strength increased from 0.001 to 0.1 mol L^{-1}. Moreover, at pH 6 and 8, increasing phosphate sorption was evidenced with increase in ionic strength. It is well known that anions adsorbed by outer-sphere association are strongly sensitive to ionic strength where as anions adsorbed by inner-sphere association either show little sensitivity to ionic strength or greater phosphate adsorption with increasing ionic strength [31]. Based on this finding, it can be concluded that phosphate anions may be specifically adsorbed on the Fe–Al binary oxide nanosorbent via forming inner-sphere surface complexes.

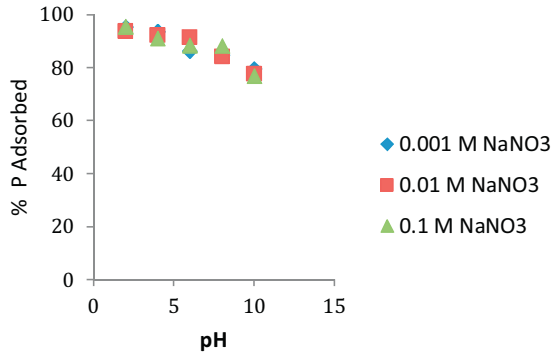

Fig. 5. Effect of ionic strength on phosphate sorption by Fe-Al binary oxide nanosorbent (initial phosphate concentration 5 mg/L and adsorbent load 0.1 g/L).

3.6. Optimum conditions

Batch mode of adsorption was conducted to optimize parameters such as adsorbent dose, speed of agitation, contact time and initial phosphate concentration and the respective optimum values were found to be pH 4; adsorbent dose 0.1 g; agitation speed 140 rpm; contact time 12 h and initial phosphate concentration 20 mg/L (data presented on the supplementary information Figs. S1–S4). Here we report the effect of pH as it is one of the most important factors that influences most adsorption processes. pH effect on the extent of phosphate adsorption onto Fe-Al binary oxide nanosorbent was investigated by varying the pH from 2 to 9 keeping the other parameters constant. The result obtained as such is illustrated in Fig. 6. In general, the sorption capacity was found to be above 97% up to pH = 7, the maximum being 99.2% at pH = 4, indicating that the Fe-Al binary oxide nanosorbent can work with a relatively wide range of pH (pH = 2–7). However, a decreasing trend in phosphate sorption was observed when the pH value exceeds 4 the decline being significant beyond pH = 7 [43]. Thus phosphate sorption would become more favorable at a lower pH than at a higher pH. The phosphate dissociation equilibrium in aqueous solution is dependent on pH which could be represented as:

$$H_3PO_4 \overset{pk1}{\rightleftarrows} H_3PO_4^- + H^+ \overset{pk2}{\rightleftarrows} H_3PO_4^{2-} + H^+ \overset{pk3}{\rightleftarrows} PO_4^{3-} + H^+$$

Where pK_1=2.15, pK_2 = 7.2 and pK_3 = 12.33 respectively. In the pH range investigated (pH = 2–9), negatively charged $H_2PO_4^-$ and $H_2PO_4^{2-}$ are the dominated species of phosphate. It can be assumed that the $H_2PO_4^-$ ions are the predominant species in the pH range of 3–6, while the HPO_4^{2-} ions appear to be the more dominant species at higher pH values. Reports indicate that the

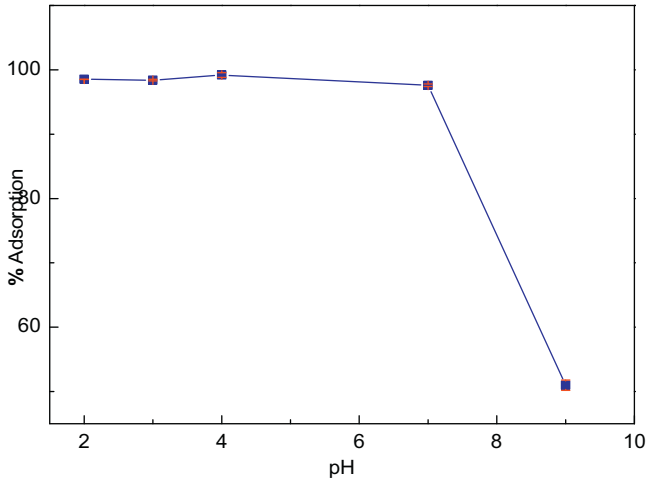

Fig. 6. Effect of pH on the removal efficiency of the nano sized sorbent for phosphate (Phosphate concentration = 30 mg/L, adsorbent dose = 0.1 g; agitation speed = 120 rpm and contact time = 24 h).

Table 2
Phosphate adsorption isotherms on Fe-Al binary oxide nanosized adsorbent.

Initial concentration(Co) mg/L	Dose of adsorbent (g)	Final concentration (Ce) mg/L	Adsorption capacity) (q_e) mg/g	C_e/q_e	Log C_e	Log q_e
20	0.1	0.028	4.99	0.0056	−1.55	0.698
30	0.1	0.337	7.41	0.045	−0.472	0.869
50	0.1	3.79	11.55	0.328	0.578	1.063
100	0.1	40.44	14.89	2.72	1.61	1.170
150	0.1	86.21	15.95	5.4	1.94	1.200
200	0.1	134.5	16.38	8.21	2.13	1.210

$H_2PO_4^-$ species are more easily adsorbed on metal (hydr) oxide surfaces than other species [41,46]. Low pH is beneficial for the surface protonation of the metal oxide. Increased protonation would increase the positively charged sites, enlarging the attraction force existing between the metal oxide surface and the negatively charged anions. Hence, higher adsorption capacity of phosphate on the sorbent was observed in the low pH region. The significant decrease in phosphate adsorption above pH 7 could be attributed to a change in surface charge caused by the nanosized mixed oxide adsorbent which is actually becoming more negative at higher pH values. This process would therefore result in the electrostatic repulsion between the exchange sites and the incoming phosphate ions [43–47]. As a result, phosphate adsorption dropped remarkably.

3.7. Adsorption equilibrium

Experiments on phosphate adsorption isotherm were conducted with different initial concentration of phosphate at room temperature keeping all other parameters at optimum conditions. The results of phosphate adsorption isotherm on the nanosized adsorbent are illustrated in Table 2.

From the linear Langmuir adsorption model,

$$\frac{C_e}{q_e} = \frac{1}{Q_o b} + \frac{C_e}{Q_O} \tag{10}$$

The plot C_e/q_e vs. C_e yields a straight line with a slope $1/Q_o$ and an intercept $1/Q_o b$. According to Fig. 7a, the slope can be read as 0.061, which reflects a Q_o value of 16.39 mg/g. Furthermore, the plot has intercept of 0.0867 which in turn gives b value of 0.7. The feasibility of the isotherm can be tested by calculating the dimensionless constant, R_L expressed as:

$$R_L = \frac{1}{1 + bC_o} \tag{11}$$

As can be seen in Table 3, R_L values are in between 0 and 1 indicating a favorable adsorption. This means that phosphate ions in solution have tended to be adsorbed on the Fe-Al binary oxide nanosorbent. The Freundlich equation is an empirical expression that encompasses the heterogeneity of the surface and the exponential distribution of sites and their energies. The linearized form of the equation is:

$$\log q_e = \log k_f + \frac{1}{n}\log C_e \tag{12}$$

Plotting log q_e versus log C_e provides a straight line with a slope of 1/n and intercept of log K_f. According to Fig. 7b, the slope value of 0.1406 could be related to the '1/n' in the Freundlich's equation.The intercept (log K_f) could be rearrenged to give value of K_f as 8.63. Therfore, a Freundlich's equation for the adsopriton process has been developed as:

$$q_e = 8.63C^{0.1406} \tag{13}$$

The value of 1/n lying between 0 and 1, which in this case is 0.1406, and the n value lying between 1 and 10, which in this case is 7.11, indicate a favorable condition for adsorption [39]. The Langmuir's and Freundlich's curves were interpreted with respect to correlation coefficient (R^2), a statistical measure of how well the regression line approximates the real data point (Table 4). In this study, the sorption isotherm of the Fe-Al binary oxide nanosorbent showed better fit to both isotherms though the value of R^2 is relatively higher for Langmuir's equation than the Freundlich (i.e.

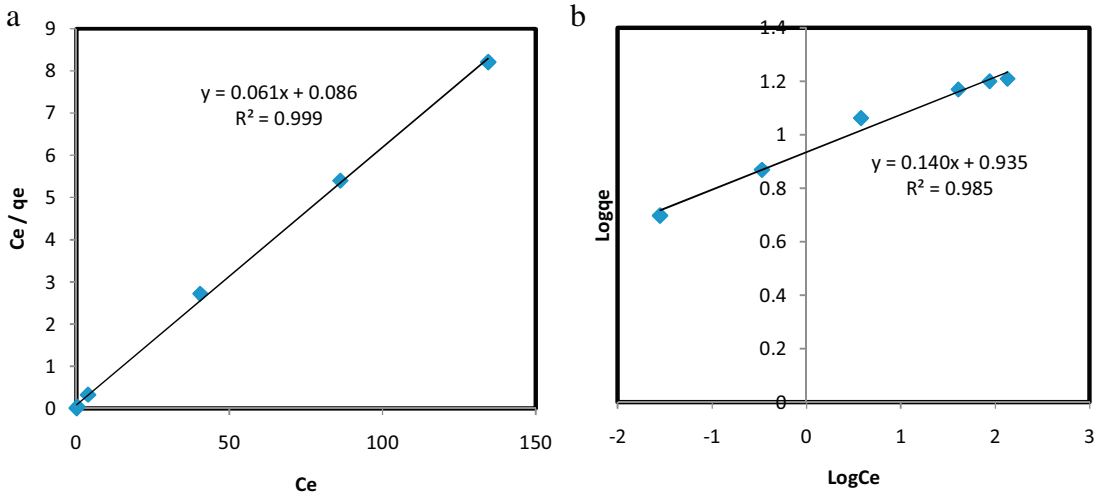

Fig. 7. a) Langmuir adsorption isotherms for phosphate adsorption and b) Freundlich adsorption isotherm for phosphate adsorption.

Table 3
R_L values for phosphate adsorption at different concentration.

Initial concentration (mg/L	20	30	50	100	150	200
R_L	0.066	0.045	0.027	0.014	0.009	0.007

Table 4
Langmuir and Freundlich constants for phosphate removal onto Fe-Al binary oxide. Nanoadsorbent

Langmuir isotherm model				Freundlich isotherm model		
Q^0	b	R_L	R^2	K_f	1/n	R^2
16.39	0.7	0.066	0.9992	8.63	0.1406	0.985

0.999 versus 0.985, respectively). This indicates that each sites of the adsorbent can accommodate one molecule of phosphate ion or can be characterized by supporting surfaces of different affinity (heterogeneity of surfaces which may be from doping of aluminum). Comparison of the maximum adsorption capacity of the Fe-Al binary oxide with other binary or ternary systems previously reported showed that the as-synthesized nanosorbent exhibited moderate sorption capacity (Table 5).

3.8. Selectivity of phosphate adsorption

Fig. 8 shows the influence of various anions on phosphate removal efficiency of Fe-Al binary oxide nanosorbent. At optimum condition, the adsorption efficiency was found to be 99.86%. In line with this, Fig. 8 shows that the adsorbent is still efficient in removing phosphate from aqueous system. It is only in the presence of fluoride ion that the adsorption efficiency decreased down to 97.68%. Evidence has been reported demonstrating the interaction between fluoride and nano alumina moieties is a feasible process [48]. Such interaction might be the reason for the decrease in adsorption efficiency of nano-sized Fe-Al binary oxide nanosorbent toward phosphate ion in the presence of fluoride.

3.9. Thermodynamic study

The thermodynamic parameters such as change in standard free energy (ΔG), enthalpy (ΔH) and entropy (ΔS) can be calculated by using the following equation:

$$\ln K_c = \frac{\Delta S}{R} - \frac{\Delta H}{TR} \quad (14)$$

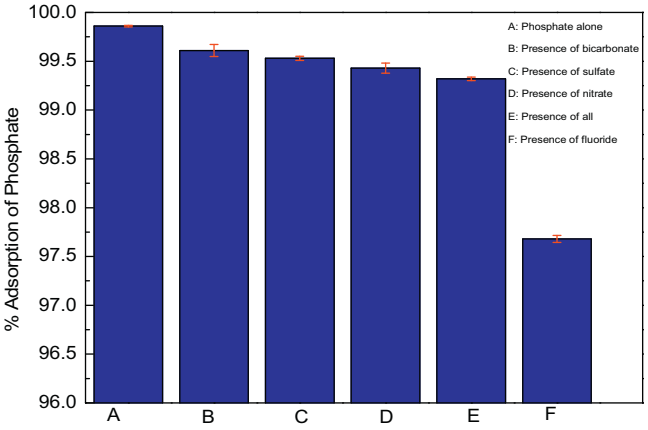

Fig. 8. Effect of co-existing anions on phosphate removal.

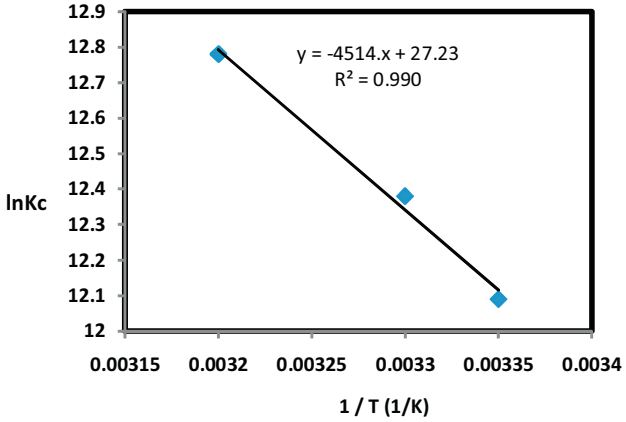

Fig. 9. Plot of lnKc vs T^{-1} for phosphate adsorption onto Fe-Al binary oxide nanosorbent (pH = 4, dose = 0.1 g, Agitation speed = 140 rpm, Contact time = 12 h, Co = 20 mg/L).

$$\Delta G = \Delta H - T\Delta S \quad (15)$$

where R (8.314J/mol K) is the gas constant, T (K) is the absolute temperature and Kc is the standard thermodynamic equilibrium constant defined by q_e/Ce. By plotting the graph of lnKc versus T^{-1} (Fig. 9), the value of ΔH and ΔS can be estimated from the slopes and intercept. ΔH and ΔS have been calculated from slope and

Table 5
Comparison of maximum phosphate adsorption capacities for different binary/ternary metal oxide adsorbents.

Adsorbents	Crystallinity	Optimum pH	Maximum Sorption Capacity mg/g	References
Fe-Mn	Amorphous	5.6	36	[1]
Fe-Zr	Crystalline	4	13.65	[18]
Fe-Al	Amorphous	3	61.5	[28]
Fe-Cu	Amorphous	7	35.2	[29]
Fe–Cu	Amorphous	5.0	39.8	[29]
Fe-Mn	Amorphous	5	123	[30]
Fe-Ti	Amorphous	6.8	35.4	[31]
Fe-Zr (magnetite)	Amorphous	3	39.1	[33]
Fe-Al-Mn	Amorphous	6.8	48.3	[49]
Ce-Zr	Crystalline	2–6	112.3	[50]
Fe-Cr	–	4	6.5	[51]
Ti-Fe	Crystalline	5	30.3	[52]
Fe-Mg-La	Amorphous	6	415.2	[53]
Fe-Al	Crystalline	4	16.4	Present Study

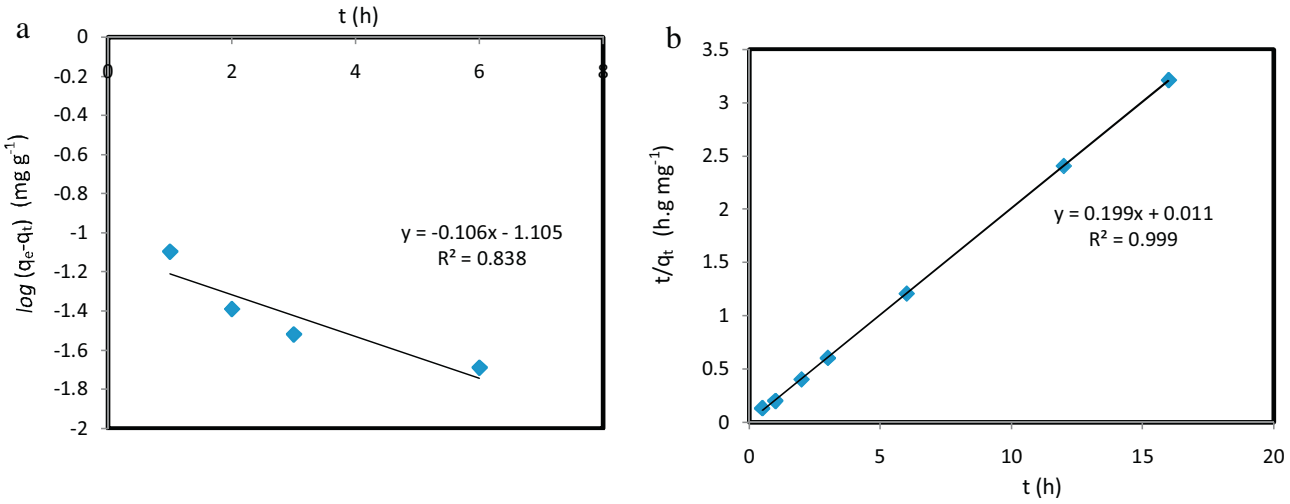

Fig. 10. Pseudo first order kinetics (a) and (b) Pseudo second order kinetics for phosphate adsorption on to Fe-Al binary oxide nanoadsorbent.

intercept of Fig. 8 as +37.53 KJ/mol and +226.39 J/mol K respectively (Table 6).

The negative value of ΔG and positive value of ΔH obtained indicated that the phosphate adsorption process is a spontaneous and endothermic process. The decrease in ΔG with increase in temperature indicated more efficient adsorption at higher temperature (308 K). The positive value of ΔS suggested that the increased randomness at the solid/solution interface occur in the internal structure of phosphate removal onto nanosized mixed oxide sorbent.

3.10. Kinetic study

The rate of the phosphate sorption onto Fe-Al binary oxide nanosorbent was studied in batch experiments at optimized values of the parameters. The kinetic data of phosphate adsorption was fitted with pseudo-first-order and pseudo-second-order models. The obtained kinetic model parameters by linear regressions are given in Fig. 10a and b and Table 7. It was found that the kinetic data at the two initial phosphate concentrations were fitted better by the pseudo-second-order adsorption kinetic rate model, indicating that chemisorption or chemical bonding between adsorbent active sites and phosphate might dominate the adsorption process [1].

3.11. Desorption study

Phosphate desorption was conducted by using the residual solids retained on the filter paper. Desorption of Phosphate from phosphate loaded adsorbents increased with increasing initial pH (Fig. 11). When the pH value is 2 the desorbed value of phosphate could not be detected. The desorbability of phosphate increased with increasing pH value. The results of this finding indicated that phosphate adsorption onto the nanosized adsorbent is not completely reversible and phosphate can be desorbed from the adsorbent by adjusting the pH value. The percent desorbed, however, in our case was relatively lower than previous reports [9,30], perhaps because we employed relatively lower volume of NaOH to effect the desorption.

4. Conclusions

The nanosized iron aluminum mixed oxide was tested to remove phosphate ions from aqueous solutions. The X-ray diffraction pattern indicated that all the as-synthesized materials are in the nano range whose particle size increased with increasing temperature. Doping of aluminum was found to delay the crystallinity of the as-synthesized compounds. The smallest particle size (20.94 nm), was found to be the 10% aluminum doped iron oxide calcinated at 300 °C (10Al300). The mechanism of phosphate adsorption was studied both from macroscopic and microscopic perspectives and both methods support the chemisorptions process as the dominant mechanism of adsorption. The effect of pH on the adsorption of phosphate showed that removal efficiency decreased with increasing pH. The optimum pH for the removal of phosphate was found to be 4. Having all the parameters optimized, this study has shown 99.86% efficiency of phosphate ion removal from aqueous solution. The adsorption processes were fitted to both Langmuir and Freundlich isotherms with the latter being higher for a wide range of adsorbate concentrations. Values of the equilibrium parameter (R_L) from Langmuir isotherm and n values from the Freundlich isotherm have indicated that the adsorption process is favorable. Thermodynamic study on the phosphate sorption process revealed that the phosphate sorption process was found to be spontaneous and endothermic. Furthermore, Phosphate desorbability was observed to increase with

Table 6
Thermodynamic parameters for phosphate adsorption on to Fe-Al binary oxide nano-adsorbent.

T(K)	ΔG(KJ/mol)	ΔH(KJ/mol)	ΔS (J/mol K)
298	−29.93	+37.53	+226.39
303	−31.06		
308	−32.19		

Table 7
Kinetic parameters for phosphate sorption onto the Fe-Al binary oxide nanoadsorbent.

First Order Model			Second Order Model		
K_1(h^{-1})	q_e (mg g^{-1})	R^2	k_2 (g h^{-1} mg^{-1})	q_e (mg g^{-1})	R^2
0.244	0.078	0.838	0.36	5.025	0.999

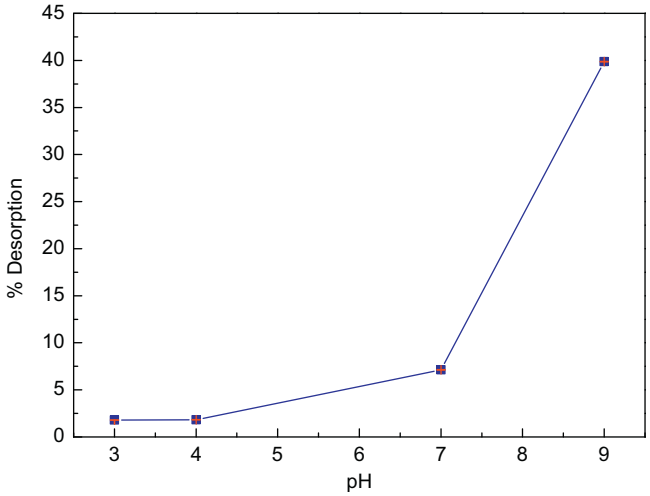

Fig. 11. Effect of pH on desorption of phosphate at varied pH.

increasing pH indicating the relatively favorable conditions for recyclability of the process at higher pH values.

Acknowledgements

The financial support from Research and Extension Office of Haramaya University, the School of Graduate Studies and Chemistry Department of HU are acknowledged. University of Cape Town is also acknowledged for running the XRD of our samples.

Appendix A. Supplementary data

Supplementary data associated with this article can be found, in the online version, at http://dx.doi.org/10.1016/j.jece.2016.04.023.

References

[1] G. Zhang, H. Liu, R. Liu, J. Qu, Removal of phosphate from water by Fe-Mn binary oxide adsorbent, J. Colloids Interface Sci. 335 (2009) 168–174.
[2] X.J. Wang, S.Q. Xia, L. Chen, J.F. Zhao, N.J. Renault, J.M. Chovelon, Nutrients removal municipal wastewater by chemical precipitation in a moving bed biofilm reactor, Process Biochem. 41 (2006) 824–828.
[3] A. Ohmen, P.C. Lemos, G. Carvallho, Z.G.J. Yuan Keller, L.L. Blackal, M.A.M. Reis, Advances in enhanced biological phosphorous removal: from micro and macro scale, Water Res. 41 (2007) 2271–2300.
[4] Y. Fukumoto, K. Haga, Advanced treatment of swine wastewater by electrodialysis with a tubular ion exchange membrane, Anim. Sci. J. 75 (2004) 479–485.
[5] N.I. Chubar, V.A. Kanibolotskyy, V.V. Strelko, G.G. Gallios, V.F. Samanidou, T.O. Shaposhnikova, V.G. Milgrandi, I.Z. Zhuravlve, Adsorption of phosphate on novel inorganic ion exchangers, Colloids Surf. A 255 (2005) 55–63.
[6] L.E. de-Bashan, Y. Bashan, Recent advances in removing phosphorus from wastewater and its future use as fertilizers (1997–2003), Water Res. 38 (2004) 4222–4246.
[7] H. Yin, Y. Yun, Y. Zhang, C. Fan, Phosphate removal from wastewater by a naturally occurring, calcium-rich sepiolite, J. Hazard. Mater. 198 (2011) 362–369.
[8] Y. Li, C. Liu, Z. Luan, X. Peng, C. Zhu, Z. Chen, Z. Zhang, J. Fan, Z. Jia, Phosphate removal from aqueous solutions using raw and activated carbon and fly ash, J. Hazard. Mater. B 137 (2006) 374–383.
[9] G. Li, S. Gao, G. Zhang, X. Zhang, Enhanced adsorption of phosphate from aqueous solution by nanostructured iron(III)–copper(II) binary oxides, Chem. Eng. J. 235 (2014) 124–131.
[10] S. Karaca, A. Gurses, M. Edjer, M. Acikyildiz, Adsorptive removal of phosphate from aqueous solutions using raw and calcinated dolomite, J. Hazard. Mater. B 128 (2006) 273–279.
[11] K. Karageorgiou, M. Paschalis, G.N. Anastassakis, Removal of phosphate species from solutions by adsorption onto calcite used as natural adsorbent, J. Hazard. Mater. A139 (2007) 447–452.
[12] F. Gérard, Clay minerals, iron/aluminum oxides, and their contribution to phosphate sorption in soils—a myth revisited, Geoderma 262 (2016) 213–226.
[13] W. Huang, S. Wang, Z. Zhu, L. Li, X. Yao, V. Rudolph, F. Haghseresht, Phosphate removal from wastewater using red mud, J. Hazard. Mater. 158 (2008) 35–42.
[14] J. Yan, D.W. Kirk, C.Q. Jia, X. Liu, Sorption of aqueous phosphorus onto bituminous and lignitous coal ashes, J. Hazard. Mater. 148 (2007) 395–401.
[15] A.O. Babatunde, Y.Q. Zhao, Equilibrium and kinetic analysis of phosphorus adsorption from aqueous solution using waste alum sludge, J. Hazard. Mater. 184 (2010) 746–752.
[16] A.H. Caravelli, E.M. Contreras, N.E. Zaritzky, Phosphorus removal in batch systems using ferric chloride in the presence of activated sludges, J. Hazard. Mater. 172 (2010) 199–208.
[17] S. Wang, C. Cheng, Y. Tzou, R. Liaw, T. Chang, J.H. Chen, Phosphate removal from water using lithium intercalated gibbsite, J. Hazard. Mater. 147 (2007) 205–212.
[18] F. Long, J. Gong, G.M. Zeng, L. Chen, X. Wang, J. Deng, Q. Niu, H. Zhang, X. Zhang, Removal of phosphate from aqueous solution by magnetic Fe-Zr binary oxide, Chem. Eng. J. 171 (2011) 448–455.
[19] H. Liu, X. Sun, C. Yin, C. Hu, Removal of phosphate by mesoporous ZrO_2, J. Hazard. Mater. 151 (2008) 616–622.
[20] O.R. Harvey, R.D. Rhue, Kinetics and energetic of phosphate sorption in a multicomponent Al(III)-Fe(III) hydr (oxide) sorbent system, J. Colloids Interface Sci. 322 (2008) 384–393.
[21] J. Lalley, C. Han, X. Li, D.D. Dionysiou, M.N. Nadagouda, Phosphate adsorption using modified iron oxide-based sorbents in lake water: kinetics, equilibrium, and column tests, Chem. Eng. J. 284 (2016) 1386–1396.
[22] S. Mustafa, M.I. Zaman, S. Khan, pH effect on phosphate sorption by crystalline MnO_2, J. Colloid Interface Sci. 301 (2006) 370–375.
[23] Y. Liu, X. Sheng, Y. Dong, Y. Ma, Removal of high-concentration phosphate by calcite: effect of sulfate and pH, Desalination 289 (2012) 66–71.
[24] S. Mustafa, M.I. Zaman, S. Khan, pH effect on phosphate sorption by crystalline MnO_2, J. Colloid. Interface Sci. 301 (2006) 370–375.
[25] S. Mustafa, M.I. Zaman, S. Khan, Temperature effect on the mechanism of phosphate anions sorption by β-MnO_2, Chem. Eng. J. 141 (2008) 51–57.
[26] H.A.B. Potter, R.N. Yong, Influence of iron/aluminum ratio on the retention of lead and copper by amorphous iron-aluminum oxides, Appl. Clay Sci. 14 (1999) 1–26.
[27] D. Dong, Y.M. Nelson, L.W. Lion, M.L. Schuler, W.C. Ghiorse, Adsorption of Pb and Cd onto metal oxides and organic material in natural surface coatings as determined by selective extractions: new evidence for the importance of Mn and Fe oxides, Water Res. 34 (2000) 427–436.
[28] A.F. de Sousa, T.P. Braga, E.C. Chagas Gomes, A. Valentini, E. Longhinotti, Adsorption of phosphate using mesoporous spheres containing iron and aluminum oxide, Chem. Eng. J. 210 (2012) 143–149.
[29] G. Li, S. Gao, G. Zhang, X. Zhang, Enhanced adsorption of phosphate from aqueous solution by nanostructured iron(III)–copper(II) binary oxides, Chem. Eng. J. 235 (2014) 124–131.
[30] J. Lu, H. Liu, X. Zhao, W. Jefferson, F. Cheng, J. Qu, Phosphate removal from water using freshly formed Fe–Mn binaryoxide: adsorption behaviors and mechanisms, Colloids Surf. A 455 (2014) 11–18.
[31] J. Lu, D. Liu, J. Hao, G. Zhang, B. Lu, Phosphate removal from aqueous solutions by a nano-structured Fe?Ti bimetal oxide sorbent, Chem. Eng. Res. Des. 93 (2015) 652–661.
[32] L. Chen, B.Y. He, S. He, T.J. Wang, C.L. Su, Y. Jin, Fe-Ti oxide nanosorbent synthesized by co-precipitation for fluoride removal from drinking water and its adsorption mechanism, Powder Technol. 227 (2011) 3–8.
[33] A. Sarkar, S.K. Biswas, P. Pramanik, Design of a new nanostructure comprising mesoporous ZrO_2 shell and magnetite core (Fe_3O_4@mZrO_2) and study of its phosphate ion separation efficiency, J. Mater. Chem. 20 (2010) 4417–4424.
[34] F.B. Li, X.Z. Li, C.S. Liu, T.X. Liu, Effect of alumina on photocatalytic activity of iron oxides for bisphenol A, J. Hazard. Mater. 149 (2007) 199–207.
[35] E.A. El-Sharkawy, S.A. El-Hakam, S.E. Samra, Effect of thermal treatment on the various properties of iron(III)-aluminum(III) coprecipitated hydroxide system, Mater. Lett. 42 (2000) 318–331.
[36] J.Y. Park, Y. Lee, P.K. Khanna, K. Jun, J.W. Bae, Y.H. Kim, Alumina-supported iron oxide nanoparticles as Fischer-Tropsch catalysts: effect of particle size of iron oxide, J. Mol. Catal. A 323 (2010) 84–90.
[37] K. Gupta, S. Bhattacharya, D. Chattopadhyay, A. Mukhopadhyay, H. Biswas, J. Dutta, N. Ranjan Ray, U.C. Ghosh, Ceria associated manganese oxide nanoparticles: synthesis, characterization and arsenic(V) sorption behavior, Chem. Eng. J. 172 (2011) 219–229.
[38] F. Gulshan, Y. Kameshima, A. Nakajima, K. Okada, Preparation of alumina–iron oxide compounds by gel evaporation method and its simultaneous uptake properties for Ni^{2+}, NH_4^+ and $H_2PO_4^-$, J. Hazard. Mater. 169 (2009) 697–702.
[39] R.L. Parfitt, R.J. Atkinson, Phosphate adsopriotn on goethite(α-FeOOH), Nature 264 (1976) 740–742.
[40] Y.S. Ho, Review of second-order models for adsorption systems, J. Hazard. Mater. 136 (2006) 681–689.
[41] L.A. Rodrigues, M.L.C. da silva, An investigation of phosphate adsorption from aqueous solution onto hydrous niobium oxide prepared by co-precipitation method, J. Colloids Surf. A. 334 (2009) 191–196.
[42] J. Kenkil, Analytical Chemistry for Technician, 2nd ed., Lewis publisher, 239, 1994.
[43] P. Persson, N. Nilsson, S. Sjoberg, Structure and bonding of orthophosphate ions at the iron oxide aqueous interface, J. Colloids Interface Sci. 177 (1995) 263–275.

[44] Z. Mao-Xu, D. Kui-Ying, X. Shao-Hui, J. Xin, Adsorption of phosphate on hydroxyaluminum and hydroxyiron-montmorillonite complexes, J. Hazard. Mater. 165 (2009) 645–651.
[45] Y. Xiaofang, W. Dongsheng, S. Zhongxi, T. Hongxiao, Adsorption of phosphate at the aluminum hydroxide-water interface: role of the surface acid-base properties, J. Colloids Surf. A 297 (2006) 84–90.
[46] L. Lai, Q. Xie, L. Chi, W. Gu, D. Wu, Adsorption of phosphate from water by easily separable Fe_3O_4@SiO_2 core/shell magnetic nanoparticles functionalized with hydrous lanthanum oxide, J. Colloids Interface Sci. 465 (2016) 76–82.
[47] Y. Liang-gua, X. Yuan-yuank, Y. Hai-qin, X. Xio-dong, W. Qin, D. Bin, Adsorpion of phosphate from aqueous solution by hydroxyl-aluminum, hydroxyl-iron, hydroxyl-iron-aluminum pillard bentonites, J. Hazard. Mater. 179 (2010) 244–250.
[48] S. Sairam, C.S. Meenakshi, Fluoride sorption using organic-inorganic hybrid type ion exchangers, J. Colloid Interface Sci. 333 (2009) 58–62.
[49] J. Lu, H. Liu, R. Liu, X. Zhao, L. Sun, J. Qu, Adsorptive removal of phosphate by a nanostructured Fe–Al–Mn trimetal oxide adsorbent, Powder Technol. 233 (2013) 146–154.
[50] Y. Su, W. Yang, W. Sun, Q. Li, J.K. Shang, Synthesis of mesoporous cerium–zirconium binary oxide nanoadsorbents by a solvothermal process and their effective adsorption of phosphate from water, Chem. Eng. J. 268 (2015) 270–279.
[51] C. Namasivayam, K. Prathap, Recycling Fe(III)/Cr(III) hydroxide, an industrial solid waste for the removal of phosphate from water, J. Hazard. Mater. B123 (2005) 127–134.
[52] M. D'Arcy, D. Weiss, M. Bluck, R. Vilar, Adsorption kinetics: capacity and mechanism of arsenate and phosphate on a bifunctional TiO_2–Fe_2O_3 bi-composite, J. Colloid Interface Sci. 364 (2011) 205–212.
[53] Y. Yu, J.P. Chen, Key factors for optimum performance in phosphate removal from contaminated water by a Fe–Mg–La tri-metal composite sorbent, J. Colloid Interface Sci. 445 (2015) 303–311.
[54] A. Olgun, N. Atar, S. Wang, Batch and column studies of phosphate and nitrate adsorption on waste solids containing boron impurity, Chem. Eng. J. 222 (2013) 108–119.